Eur. Phys. J. E (2013) **36**: 97
DOI 10.1140/epje/i2013-13097-8

THE EUROPEAN
PHYSICAL JOURNAL E

Regular Article

Light-induced rewiring and winding of Saturn ring defects in photosensitive chiral nematic colloids

I. Gvozdovskyy[1], V.S.R. Jampani[2], M. Škarabot[2,3], and I. Muševič[2,3,a]

[1] Institute of Physics of the National Academy of Sciences of Ukraine, Department of Optical Quantum Electronics, Prospekt Nauki 46, Kyiv, Ukraine
[2] J. Stefan Institute, Jamova 39, SI-1000 Ljubljana, Slovenia
[3] Faculty of Mathematics and Physics, University of Ljubljana, Jadranska 19, SI-1000 Ljubljana, Slovenia

Received 5 March 2013 and Received in final form 22 June 2013
Published online: 5 September 2013 –

Abstract. We study the winding and unwinding of Saturn ring defects around silica microspheres with homeotropic surface anchoring in a cholesteric liquid crystal with a variable pitch. We use mixtures of a nematic liquid crystal 5CB and various photoresponsive chiral dopants to vary the helical pitch and sense of the helical winding by illuminating the mixtures with UV or visible light. Upon illumination, we observe motion of the Grandjean-Cano disclination lines in wedge-like cells. When the line touches the colloidal particle, we observe topological reconstruction of the Grandjean-Cano line and the Saturn ring. The result of this topological reconstruction is either an increase or decrease of the degree of winding of the Saturn ring around the colloidal particle. This phenomenon is similar to topological rewiring of $-1/2$ disclination lines, observed recently in chiral nematic colloids.

1 Introduction

Liquid crystals doped with various colloidal particles and nanoparticles have attracted a lot of attention in recent years. The interest is driven because of high potential to create novel composite materials with interesting properties as well because of fundamental topological phenomena and colloidal interactions. When foreign particles are added to the homogeneously oriented nematic liquid crystal (NLC), then the topological defects in the form of points or loops are observed around the particles [1–4], depending on the nature of the surface anchoring of the NLC. Topological defects always accompany colloidal particles and are responsible for novel colloidal interactions of different complexity, which cannot be observed in water-based colloids. Most complex interaction that was observed in nematic colloids, are topologically entangled colloidal states, such as, for example, figure of eight, figure of omega, as well as knotted and linked chiral nematic colloids [5–9].

It is well known that adding small amounts of chiral dopants (ChD) to the nematic liquid crystal results in the formation of the cholesteric liquid crystal (CLC) that is characterized by helical structure with the helical pitch p. The twisting sense of the cholesteric helix can be right- or left-handed, depending upon the nature of ChDs and their interaction with molecules of the nematic LC [10]. In the planar CLC texture with the helical axis perpendicular to the surface of the LC cell, a helical structure selectively reflects light in a narrow spectral range according to Bragg's law [10]. The length of the helical pitch can be influenced by temperature, light, external electrical and magnetic fields, which is the basis for various applications of CLCs in displays, thermal sensors, polarizers, mirrorless lasers, etc. [11–16]. Recent studies of photosensitive chiral molecules and their influence on the structure and properties of CLCs have attracted great attention because of practical applications as light-driven molecular switches or motors [17–21] and other devices [22–27]. Photonic manipulation of molecules that provide the alignment of liquid crystals on the surfaces of colloidal particles was used to transform nematic colloids between different topological states [28, 29].

Recently, an experimental and theoretical study of the nature of defect loops, winding around spherical colloidal particles in the CLC was presented [9]. Silica colloidal microsphere with the diameter $20\,\mu$m with homeotropic surface anchoring were dispersed in a planar texture of right-handed CLC (nematic 5CB doped by right-handed ChD CB15) for various lengths of helical pitches and therefore variable ratio of the helical pitch p to the colloidal diameter $2R$. If the CLC is photosensitive, then its helical pitch p and the twisting sense of the cholesteric helix can be controlled by light due to

[a] e-mail: igor.musevic@ijs.si

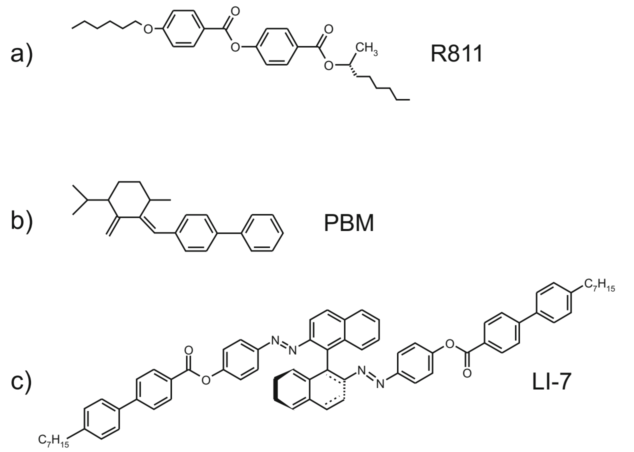

Fig. 1. Molecular structures of chiral dopants.

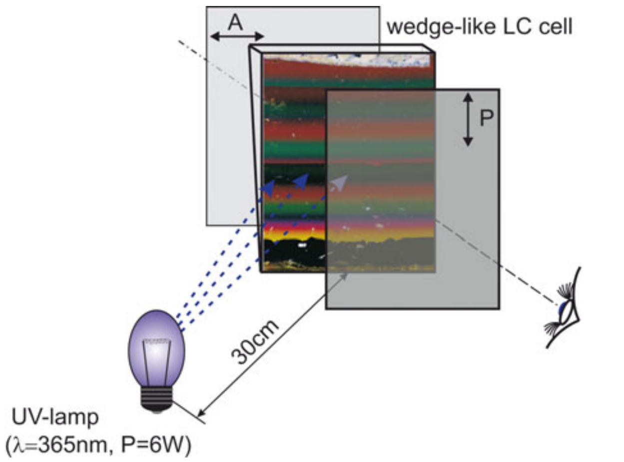

Fig. 2. Set up for illumination of the two-component chiral nematic mixture and observation of Grandjean-Cano textures.

the photoinduced change in the conformation of ChD or nematic LC [30–35]. The changes of pitch and twisting sense of the homeotropically alignment cholesteric mixture based on two ChDs with opposite chiralities (photosensitive left-handed 2-(4′- phenylbenzylidene)-p-menthane-3-one (PBM) and non-photosensitive right-handed R811) were also studied [25,36].

Here we report the first study of photosensitive cholesteric colloids, based on two-component cholesteric mixture of left-handed PBM and right-handed R811 doped with spherical silica particles with diameter 20 μm. We study the time-development of defect loops around a single colloidal particle in the cholesteric planar cell during the UV irradiation. The UV light gradually induces the change of the chiral nematic twisting angle from 3π to π through the compensated nematic phase and vice versa. Planar CLC texture therefore evolves from the starting left-handed cholesteric (LHC) through the chirality-compensated nematic phase (N) to the final, right-handed cholesteric (RHC) structure [36].

2 Experiment

Two chiral mixtures were prepared to study photosensitive chiral nematic colloids. To realize an irreversible left-handed cholesteric-nematic-right-handed cholesteric (LHC-N-RHC) structural transitions we used the right-handed ChD ZLI-3786 (R811, Licrystal, Merck) and the left-handed ChD 2-(4′-phenylbenzylidene)-p-menthane-3-one (PBM) synthesized at the Institute for Single Crystals, NAS of Ukraine [31]. To study chiral colloids with reversible LHC-N-RHC structural transition, the right-handed R811 and the photosensitive left-handed ChD LI-7, synthesized at Liquid Crystal Institute & Chemical Physics Program, Kent State University, were used [26, 37]. Molecular structures of chiral molecules are shown in fig. 1.

Right-handed or left-handed chiral dopants were dissolved in the nematic LC 4-cyano-4′-pentylbiphenyl (5CB, Nematel) at various concentrations to determine their helical twisting power. The two-component cholesteric mixtures were prepared using two ChDs with opposite chiralities to realize a photosensitive LHC-N-RHC structural transition. The starting concentration of ChDs was selected so that the twisting angle of the CLC over the cell thickness was 3π ($p \cong 15\,\mu$m). To measure the cholesteric pitch we used well-known Grandjean-Cano method [38,39].

In our experiments spherical silica particles (Duke Scientific) with a diameter of $2R = (18 \pm 2)\,\mu$m were used. Surfaces of particles were treated with octadecyl dimethyl (3- tri methoxy silylpropyl) ammonium chloride (DMOAP, ABCR GmbH) in order to obtain strong normal surface anchoring as described in ref. [40]. Silica particles were dispersed into the two-component cholesteric mixtures and after this colloid dispersion was mixed for about 15 minutes.

To obtain planar alignment of CLC, we used polyimide PI-2555 (NISSAN Chemicals, Japan). The polyimide films were deposited on glass substrates with ITO electrodes by spin-coating method (5000 rpm, 30 s) and then annealed at 180 °C for 30 min. The polyimide layer was unidirectionally rubbed and wedge-like cells were assembled using these substrates with antiparallel rubbing on both aligning surfaces. The thickness of the gap was set to 25–30 μm by mylar spacers and controlled by the interference method measuring the transmission spectra of empty cells. Wedge-like cells with a wedge angle of 0.1° were filled with chiral nematic colloidal dispersions using capillary action at room temperature. Illumination of the LC cells containing two-component chiral nematic colloidal dispersions was carried out by a UV lamp (Cole Parmer Instrument Co., Vernon Hills, Illinois) as shown in fig. 2. The power of the UV radiation at $\lambda = 365$ nm was 6 W. To study reversible LHC-N-RHC structural transitions the samples were irradiated with visible light ($\lambda_{max} = 532$ nm). The Grandjean-Cano texture of the CLC was observed using crossed polarizers and images were taken by a digital camera (Nikon D80, Japan). Additionally, to estimate the helical sense of the chiral nematic mixtures for various UV exposure doses, we used Grandjean-Cano method as described previously [41].

To study the transformation of the defect loops around the colloidal particles in two-component chiral mixtures under UV radiation, a laser tweezers setup [42–47] was used to grab the defect lines and discern their topology. A laser tweezers was built around an inverted microscope (Nikon Eclipse, TE2000-U) with infrared fiber laser operating at 1.064 μm as the light source and a pair of acousto-optic deflectors driven by a computerized system (Aresis, TWEEZ 70) that were used for trap manipulation [47].

3 Results and discussion

3.1 Single-dopant cholesteric mixtures

First we studied the dependence of the cholesteric pitch on the concentration of various chiral dopants added into the nematic LC 5CB to determine their helical twisting power. The length of the cholesteric pitch p was calculated using Grandjaen-Cano method [38,39], $p = 2d/N$, where N is the number of Grandjean-Cano stripes that appear in a wedge-like cell from zero thickness to the thickness d. The dependencies of the cholesteric pitch on the concentration of various chiral dopants are shown in fig. 3a. The experimental points are shown by solid symbols. Since the concentrations of chiral dopants in the nematic 5CB are low, the dependence of the reciprocal cholesteric pitch is a linear function of the concentration, as shown in fig. 3b. From fig. 3b we determined the helical twisting power β (HTP) of chiral dopants in the nematic host 5CB, $\beta = 1/(p\mathrm{C})$. As can be seen from fig. 3b, the maximum values of HTP are $\beta = -0.71$ [μm wt.%]$^{-1}$ for left-handed LI-7 and $\beta = -0.54$ [μm wt.%]$^{-1}$ for PBM. On the other hand, the right-handed ChD R-811 has quite small HTP of $\beta = +0.14$ [μm wt.%]$^{-1}$.

3.2 Two-component cholesteric mixtures

By using previous results for single-dopant chiral mixtures, we prepared various two-component mixtures that contained two chiral dopants of opposite chiralities in order to realize the evolution from the left-handed cholesteric via the compensated nematic to the right-handed cholesteric (LHC-N-RHC) structure under the UV irradiation, as it was recently shown for homeotropic anchoring [25,34]. In the initial state the concentrations of chiral dopants are chosen so that the sign of the cholesteric helix is determined by the left-handed photosensitive chiral dopant (PBM or LI-7). Two mixtures were prepared for the study of the photosensitive chiral nematic colloids. The first mixture (M1) was prepared for the study of irreversible LHC-N-RHC structural transition. For this we used a two-component cholesteric mixture based on the photosensitive left-handed ChD PBM and right-handed ChD R811 with concentration $C_{PBM} = 1$ wt.% and $C_{R811} = 2$ wt.%, respectively. The second mixture (M2) was prepared for studies of reversible LHC-N-RHC. This mixture consists of the photosensitive left-handed ChD LI-7 and the right-handed ChD R811 with concentrations of $C_{LI\text{-}7} = 0.14$ wt.% and $C_{R811} = 2.3$ wt.%, respectively.

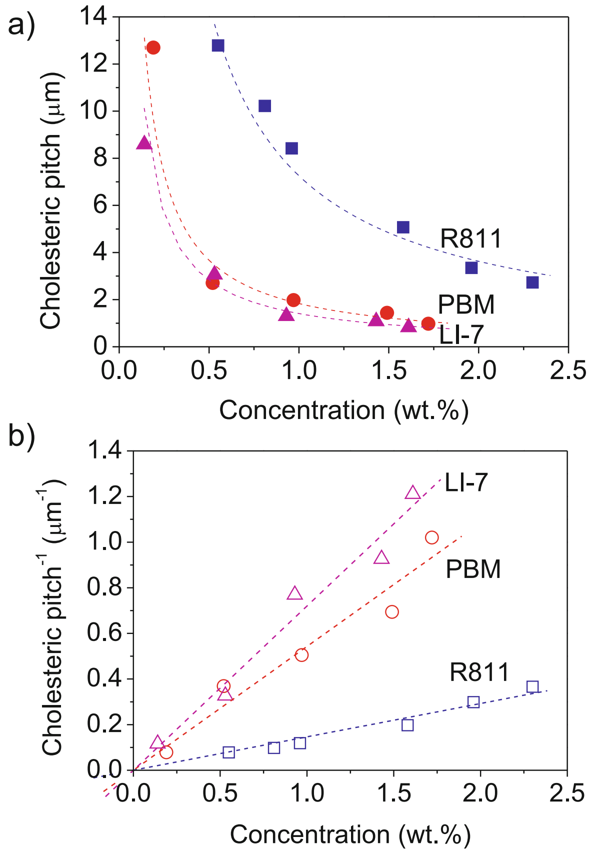

Fig. 3. (a) Dependence of the cholesteric pitch (solid symbols) and (b) reciprocal cholesteric pitch (open symbols) on the concentration of various chiral dopants (R811: squares, PBM: circles and LI-7: triangles) in the nematic LC 5CB

The cholesteric pitches of mixtures M1 and M2 were 13.3 and 12.4 μm. These values roughly correspond to 3π winding angle of the helical CLC structure across the spherical silica colloidal particles with the diameter of 20 μm.

3.2.1 UV irradiation of the two-component mixture

As mentioned above, the concentrations of the photosensitive chiral dopants are chosen so that the cholesteric helices of the two-component mixtures are left-handed at the start of each experiment. UV irradiation of mixtures M1 or M2 results in photoisomerization of chiral photosensitive dopants PBM or LI-7. Due to the *cis-trans* isomerization of the left-handed chiral dopants, the HTP of molecules is decreased and the cholesteric helix is gradually unwinding. This unwinding is observed in wedge-like cells as a gradual decrease of the number of Grandjean-Cano stripes (GC), as shown in figs. 4 (a-c). At a certain exposure dose, the HTPs of the two dopants with opposite chiralities are equal and they compensate each other, resulting in an unwound nematic (compensated nematic phase) as shown in fig. 4 d. Continuing UV irradiation of mixture M1 or M2 results in further depletion of the concentration of left-handed photosensitive ChDs. In this case, the elastic torque caused by left-handed dopants becomes weaker

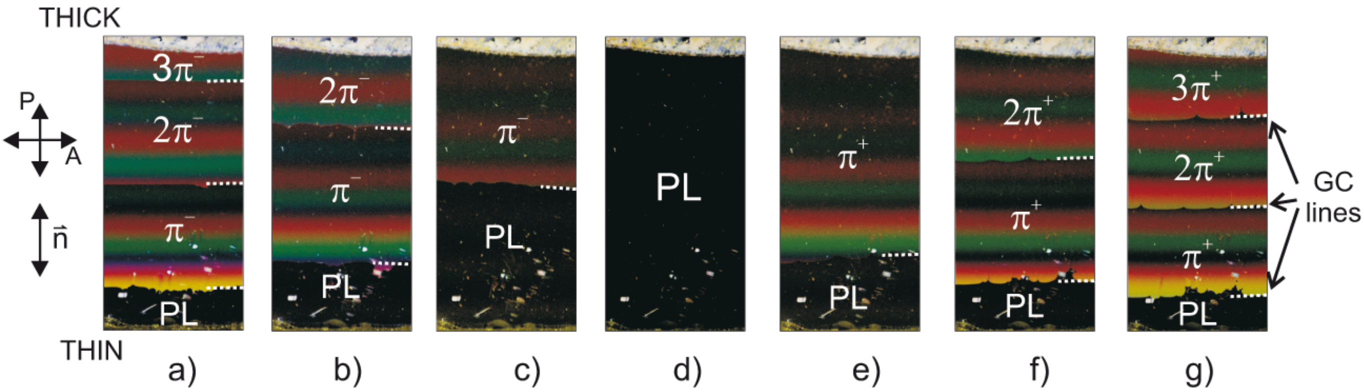

Fig. 4. The LHC-N-RHC structural transition under UV irradiation in wedge-like cell filled with M1, observed between crossed polarizers. (a-c) Unwinding of the left-handed cholesteric helix; d) compensated cholesteric phase; (e-g) winding of the right-handed cholesteric helix.

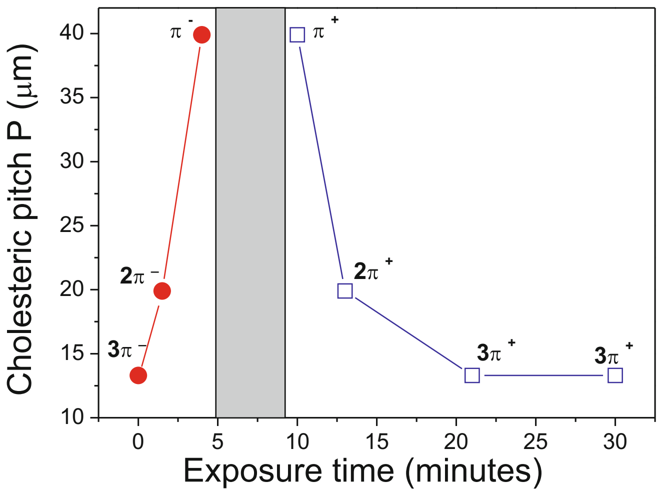

Fig. 5. Dependence of the pitch length on the exposure time for two-component chiral mixture M1. Solid symbols correspond to the left-handed cholesteric helix and open symbols denote the right-handed cholesteric helix. The gray area corresponds to the unwound state of the chiral mixture M1.

than that of the right-handed dopant (R811), which leads to the formation of the right-handed helix and gradual increase of N with prolonged irradiation, as can be seen from figs. 4 (e-g). Dependence of the cholesteric pitch on the exposure time for cholesteric mixture M1 is shown in fig. 5. Under UV radiation (t_{exp} = 0–5 min) the unwinding of initial left-handed cholesteric helix (solid circles) is observed. Cholesteric pitch of the mixture increases from $p = 13.3\,\mu$m to $p = 39.9\,\mu$m. Further exposition leads to the LHC-N transition. The unwound state is formed in a wide range of exposure doses (t_{exp} = 5–10 min), where the elastic torque is very weak and the system is not able to twist. Further irradiation of this unwound state leads to rewinding of the structure into the right-handed helix (open squares) as shown in fig. 5. Under prolonged irradiation (t_{exp} = 10–30 min) the cholesteric helix is winding and the pitch of the helix is decreased to $p = 13.3\,\mu$m.

3.3 Study of the two-component dispersion of chiral nematic colloids under UV-VIS irradiation

To study the photosensitive chiral colloids under UV irradiation we used two chiral mixtures M1 and M2. In mixture M1 we studied the changes of the topology of defect loops winding around colloidal particles for the irreversible LHC-N-RHC transition. In mixture M2 we studied in details the time-evolution of the defect loop around a single colloidal particle in π-twisted helix for the reversible LHC-N-RHC transitions.

3.3.1 Irreversible LHC-N-RHC transitions

Before the beginning of UV irradiation, wedge-like cell with maximum thickness $d = 25\,\mu$m were filled with the left-handed chiral mixture M1 with initial cholesteric pitch $p = 13.3\,\mu$m. Upon UV irradiation, a continuous unwinding of the defect loop around a selected silica microsphere with homeotropic surface anchoring is observed (fig. 6), similar to the observations in ref. [9], where cells with different and fixed chirality were used. Under UV irradiation the cholesteric helix is gradually unwound from the initial pitch $p = 13.3\,\mu$m (corresponding to 3π winding across the particle) to $p = 19.9\,\mu$m ($\sim 2\pi$). This transition is shown in fig. 6a and fig. 6b. Unwinding of the helical pitch leads to the clearly observable change of the structure of the defect loop around the colloidal particle.

Upon further illumination, unwinding of the cholesteric pitch is observed from 2π structure in fig. 6b to structure in fig. 6c ($p = 39.9\,\mu$m). This can be clearly seen from the change of the topology of the defect loop around the particle. Whereas in fig. 6b, corresponding to 2π structure, the loop is highly twisted, the defect loop in the π-structure is less twisted and forms the well-known “figure of eight” loop (fig. 6c), which was observed recently [9]. The structure of the “figure of eight” loop can easily be understood, when we consider what happens in the next step upon further irradiation, which leads to the unwound, chirality-compensated nematic phase of mixture M1. In this case the defect loop appears in form of a single Saturn ring, encircling

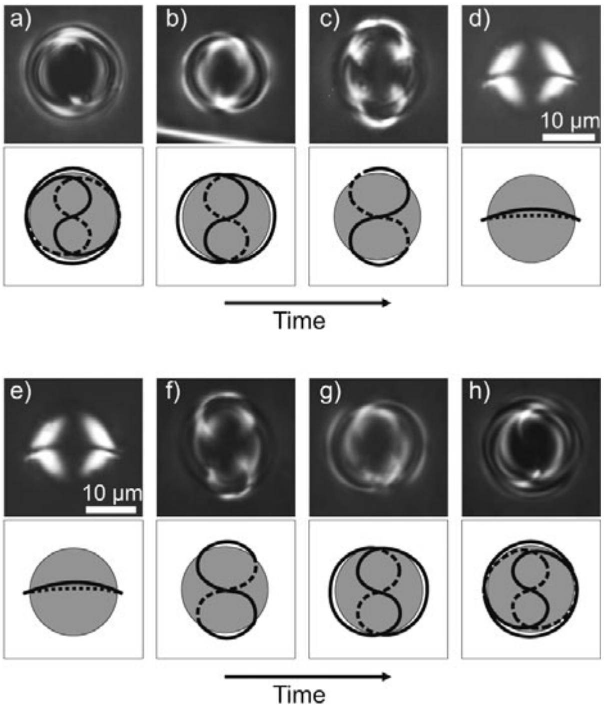

Fig. 6. A single defect loop is wound around the silica microsphere with homeotropic surface anchoring in a cell filled with M1. Under continuous UV irradiation, the pitch unwinds and then winds again. (a - d) Irreversible unwinding from LHC to N. In panels (d,e), the Saturn ring is slightly bent. (e - h) Irreversible UV light-induced winding from N to RHC.

the microsphere. As can be seen from fig. 6d this Saturn ring is lying in the plane, oriented perpendicular to the rubbing direction. We see that winding or unwinding of the cholesteric structure has a very simple effect on the Saturn ring. If we start from the Saturn ring in the chirality-compensated sample, twisting of the cholesteric structure is equivalent to rotating one of the plates with respect to the other, around the helical axis. This "winding", enforced by the plate rotation, winds the helical structure and shortens the pitch (or enlarges) and as a consequence also "twists" the Saturn ring around the helical axis.

This is actually seen upon further UV irradiation of the nontwisted state (fig. 6e). As the cholesteric structure twists, also the originally untwisted Saturn ring is twisting, and forms the figure of eight when half of the cholesteric pitch equals to the colloidal diameter and we have the twisted state, shown in fig. 6f. A more twisted defect loop is observed upon continuing irradiation, when the cholesteric pitch forms 2π-twisted and 3π-twisted Saturn ring (fig. 6g and fig. 6h, respectively).

3.3.2 Reversible LHC-N-RHC transitions

In reality, the mechanism of winding of the Saturn ring around the colloidal particle is of course different from the hypothetic model we have just described, because the two plates of the sample are fixed in real experiment and do not rotate. So how does the Saturn ring wind around the microsphere in a real cholesteric mixture, which has a variable pitch? To demonstrate this mechanism of Saturn ring winding around the silica microspheres in more detail, we used the mixture M2, which exhibits reversible LHC-N-RHC transition under UV-irradiation. We irradiate the dispersion and we take the movie, which is afterwards analyzed frame by frame.

Wedge-like cell with thickness varying from zero to $d = 25\,\mu$m was filled with a dispersion of colloidal microspheres with average diameter of $18\,\mu$m in the two-component photoresponsive cholesteric mixture M2. The initial pitch of the left-handed cholesteric helix was $12.4\,\mu$m, which corresponds to 3π winding of the defect loop around the microsphere. The UV-irradiation of photoresponsive chiral colloids at a peak wavelength $\lambda = 365\,$nm leads to the *trans-cis* isomerization of the LI-7 chiral dopant, which changes the balance of the helical twisting power of both dopants. As a result, gradual change of the cholesteric pitch from 3π-winding to fully compensated nematic phase were observed. Further UV-irradiation results in re-winding of the cholesteric phase with opposite sense of the helix. When the colloid dispersion M2 was irradiated with visible light with a peak wavelength at $\lambda = 520\,$nm, *cis-trans* isomerization of LI-7 took place and the reversible RHC-N-LHC transition was observed.

To study the winding of a defect loop around a colloidal microsphere, we choose a simple starting colloidal topology, when one-half of the cholesteric pitch is equal to the colloidal diameter 2R (π-winding) and the Saturn ring around colloid particle is twisted into the figure of eight. This is presented in panel (a) of fig. 7. In the upper part of this panel one can see the nearly horizontal defect line, which is the Grandjean-Cano disclination line, separating the two regions with different numbers of the helical half-turns. Thinner part of the sample is on top of all panels, thicker part is on the bottom side. In our case, the number of half-turns of the helical structure in the region above the disclination line is smaller by 1 compared to the region bellow the disclination line. Across this disclination line, the number of helical half-turns is therefore increased by 1 when we go from thinner (upper) part to thicker (lower) part of the wedge-like cell. A very interesting evolution of the topology of the Saturn ring defect and the Grandjean-Cano line is observed, when the cholesteric LC is illuminated and the trans-cis- isomerization of LI-7 starts to elongate the helical period. Because of this increase of the pitch length, the Grandjean-Cano disclination line starts to move towards the thicker part of the wedge-like cell. When this line touches the twisted Saturn ring, winding around the colloidal microsphere, the line and the loop are first cut and then immediately rewired into a combination of the Grandjean-Cano line with a loop, as seen in panel (b) of fig. 7. It is clearly seen from this panel that there is a single topological line, which is a merger of the Grandjean-Cano disclination line and the figure of eight line (*i.e.* twisted Saturn ring).

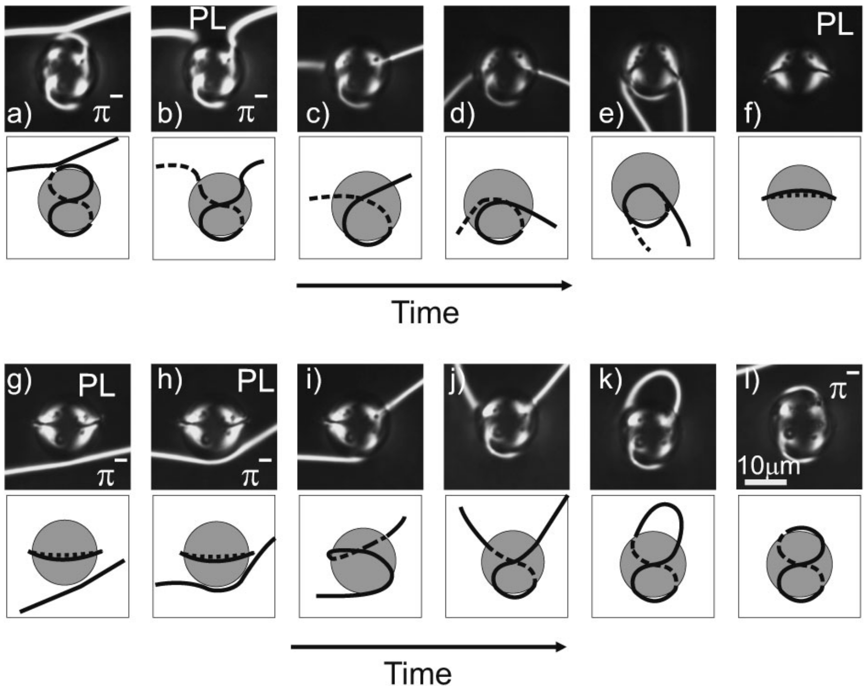

Fig. 7. The process of unwinding (under UV) and winding (under VIS-irradiation) of the Saturn ring around the colloidal particle is inherently connected to the Grandjean-Cano disclination line. (a) Grandjean-Cano line is just touching the figure-of-eight loop. (b-e) the Grandjean-Cano line and the figure of eight are cut and rewired into a simple line with a single loop. (f-g) Grandjean-Cano loop separates and leaves behind a Saturn ring. (h-l) The opposite rewiring process is observed when the helix winds again under VIS-irradiation of the photoresponsive CLC mixture. PL denotes planar nematic structure where the chirality is fully compensated. π^- denotes the twisted state, where the diameter of the colloid is equal to one half of the helical pitch.

As the UV illumination and photoisomerization of LI-7 proceed and the helical period further increases, the Grandjean-Cano line moves towards thicker part of the sample and "undresses" the cut Saturn ring from the microsphere, see panels (c-e) in fig. 7. Then, at a certain moment, the Grandjean-Cano line detaches from the Saturn ring, which remains isolated and encircles the microsphere, as shown in panel (f) of fig. 7.

We now start to illuminate the sample with VIS light, which causes reversible trans-cis isomerization and rewinding of the helical structure. The resulting topology of the Saturn ring is shown in panels (g-l) of fig. 7. The Grandjean-Cano disclination line now moves in the opposite direction, *i.e.* towards thinner part of the sample, because the helical pitch gets shorter and shorter. We see from panels (h,i) that at a certain moment, the line touches the Saturn ring, then both lines are cut and rewired into a single topological defect line with a loop. This line then moves towards the thinner part of the sample and "dresses again" the microsphere with a novel defect loop, which is the figure of eight. At a certain moment the Grandjean-Cano line detaches from the figure of eight (fig. 7k) and we end in the same situation we started with.

The question is how are the Grandjean-Cano lines topologically related to the (twisted) Saturn ring and what is the mechanism of their merging during the process of re-wiring. The topology of Saturn rings in different chiral environment and their mutual rewiring have been extensively studied in recent years [48,49]. Similarly, the nature of the Grandjean-Cano lines has been the subject of long term studies and is now well understood [50–53]. These lines are separating the regions with different degree of twist and when crossing the line, the angle of the total twist of the CLC either increases or decrease for π. Microscopy and in particular the fluorescent confocal polarizing microscopy (FCPM) observations have revealed three different types of Grandjean lines in wedge nematic cells [53]. The first type of line that separates homogeneous from the π twisted nematic is the twist disclination line. This line is of a singular character and the order parameter is ill defined in its core, resulting in the depressed degree of ordering in the core. For larger thickness, it is followed by "thin" Grandjean lines, which are the combination of a singular $\tau^{-1/2}$ (or $\tau^{+1/2}$) defect line and a non-singular (escaped) $\lambda^{+1/2}$ (or $\lambda^{-1/2}$) line. Thin lines are for larger thickness followed by "thick" lines, which are combinations of the $\lambda^{-1/2}$ and $\lambda^{+1/2}$ lines, as evidenced from confocal polarized microscopy images [53]. The nomenclature of Kleman and Friedel is used [50], where λ refers to the vector that is equivalent to the director, τ refers to the product $\tau = \lambda \times \chi$, where χ is the unit vector along the helical axis. The superscripts describe the winding number [10], well known from the topological description of defect lines and loops in nematics. The singular $\tau^{-1/2}$ line is therefore topologically equivalent to the Saturn ring and has the same internal order parameter structure.

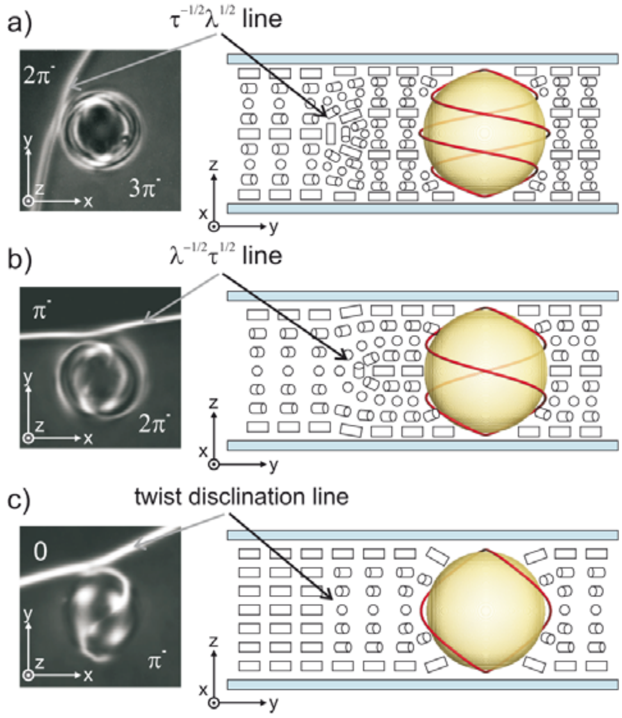

Fig. 8. Director structure in the vicinity of the Grandjean-Cano line and the colloidal particle in chiral nematic liquid crystal. (a) $3\pi^- \rightarrow 2\pi^-$ transition region. The Saturn ring is triple-twisted around the colloid and the $\tau^{-1/2}\lambda^{+1/2}$ Grandjean-Cano line separates the two differently twisted regions. (b) $2\pi^- \rightarrow \pi^-$ transition region. The Saturn ring is here double-twisted and the $\tau^{+1/2}\lambda^{-1/2}$ Grandjean-Cano is present. (c) $\pi^- \rightarrow PL$ transition region. The Saturn ring is twisted for π, and the twist disclination line separates the colloid from the planar region.

Figure 8 shows the crossed-polarizer images and the sketch of the director profiles in case when the Grandjean-Cano line is approaching the colloidal particles with the twisted Saturn ring. Three different scenarios are shown with decreasing degree of twist: the $3\pi^- \rightarrow 2\pi^-$ transition in fig. 8a, $2\pi^- \rightarrow \pi^-$ transition in fig. 8b and $\pi^- \rightarrow PL$ transition in fig. 8c. One can see the overall consistency of the nematic director field around the Grandjean-Cano lines and the twisted Saturn ring encircling the colloidal particle. In case of $3\pi^- \rightarrow 2\pi^-$ line it is energetically favorable to connect the singular $\tau^{-1/2}$ line with the $s = -1/2$ Saturn ring due to the same internal structure. In case of $2\pi^- \rightarrow \pi^-$ line the singular $\tau^{+1/2}$ line should be connected in the process of re-wiring with the $s = -1/2$ Saturn ring, meaning that a "hybrid" disclination line transiting from $+1/2$ to $-1/2$ winding number should be created. This scenario of the transiting behavior of disclination lines in nematics has in fact recently been discussed by Čopar and Žumer [54]. However, in order to prove this assumption, fluorescence confocal polarizing microscopy should be performed, which could give us a conclusive proof of this hypothetical hybrid structure of disclination lines.

4 Conclusions

Winding and unwinding of the Saturn ring around a colloidal particle in a cholesteric liquid crystal with a variable helical period is a complex topological process that can be most directly analyzed in wedge type cells filled with CLC. In these cells, elongation or contraction of the helical period result in the movement of the Grandjean-Cano lines to accommodate multiples of the half-helical period with the local thickness. We clearly demonstrated that the process of winding and unwinding of the Saturn ring is always accompanied with topological rewiring of the Cano wedge line and the Saturn ring. This process is topologically interesting, because it implies the interaction of singular $\tau^{\pm 1/2}$ lines forming the Grandjean-Cano thin lines and the $s = -1/2$ Saturn ring. This interaction could in some cases lead to the hybridization of disclination lines, where the sense of the director winding is expected to alternate along the combined Grandjean-Cano-Saturn ring line.

The authors thank Dr. W. Becker from Merck for providing chiral dopant R-811, Prof. L. Kutulya for kind provision of PBM material and Dr. Quan Li from Kent State University for providing LI-7. This work was supported by the Slovenian Research Agency (ARRS) under the project J1-3612. V.S.R.J. acknowledges support from the Marie Curie Network HIERARCHY.

References

1. P. Poulin, H. Stark, T.C. Lubensky, D.A. Weitz, Science **275**, 1770 (1997).
2. E.M. Terentjev, Phys. Rev. E **51**, 1330 (1995).
3. O. Mondain-Monval, J.C. Dedieu, T. Gulik-Krzywicki, P. Poulin, Eur. Phys. J. B **12**, 167 (1999).
4. Gu Yuedong, N.L. Abbott, Phys. Rev. Lett. **85**, 4719 (2000).
5. T. Araki, H. Tanaka, Phys. Rev. Lett. **97**, 127801 (2006).
6. S. Žumer, *21st International Liquid Crystal Conference, Keystone, Colorado, USA, July 2-7, 2006* (Kinsley & Associates, Littletown, 2006).
7. M. Ravnik, M. Škarabot, S. Žumer, U. Tkalec, I. Poberaj, D. Babič, N. Osterman, I. Muševič, Phys. Rev. Lett. **99**, 24801 (2007).
8. U. Tkalec, M. Ravnik, S. Čopar, S. Žumer, I. Muševič, Science **333**, 62 (2011).
9. V.S.R. Jampani, M. Škarabot, M. Ravnik, S. Čopar, S. Žumer, I. Muševič, Phys. Rev. E **87**, 031703 (2011).
10. P.G. de Gennes, *The Physics of Liquid Crystals* (Clarendon, Oxford, 1974).
11. D.-K. Yang, J.W. Doane, Z. Yaniv, J. Glasser, Appl. Phys. Lett. **64**, 1905 (1994).
12. B. Taheri, J.W. Doane, D. Davis, D.St. John, SID Int. Symp. Digest Tech. Papers **27**, 39 (1996).
13. Z. Li, P. Desai, R.B. Akins, G. Ventouris, D. Voloschenko, *Electrically tunable color for full-color refractive displays*, in *Liquid Crystal Materials, Devices, and Applications VIII*, edited by L.-C. Chien, Proc. SPIE, Vol. **4658** (2002) p. 7.
14. D.J. Broer, J. Lub, G.N. Mol, Nature **378**, 467 (1995).
15. L. Li, J. Li, B. Fan, Y. Jiang, S.M. Faris, Proc. SPIE-Int. Soc. Opt. Eng. **3560**, 33 (1998).

16. I.P. Ilchishin, E.A. Tikhonov, V.G. Tishchenko, M.T. Shpak, JETP Lett. **32**, 27 (1980).
17. C. Denekamp, B.L. Feringa, Adv. Mater. **10**, 1080 (1998).
18. B.L. Feringa, R.A. van Delden, N. Koumura, E.M. Geertsema, Chem. Rev. **100**, 1789 (2000).
19. K. Ichimura, Chem. Rev. **100**, 1847 (2000).
20. B.L. Feringa, J. Org. Chem. **72**, 6635 (2007).
21. Ya. Wang, Q. Li, Adv. Mater. **24**, 1926 (2012).
22. I. Terenetskaya, I. Gvozdovsky, Mol. Cryst. Liq. Cryst. **368**, 551 (2001).
23. A.Yu. Bobrovsky, N.I. Boiko, V.P. Shibaev, J. Springer, Liq. Cryst. **28**, 919 (2001).
24. M. Aronishidze, A. Chanishvili, G. Chilaya, G. Petriashvili, S. Tavzarashvili, L. Lisetski, I. Gvozdovskyy, I. Terenetskaya, Mol. Crys. Liq. Cryst. **420**, 47 (2004).
25. I. Gvozdovskyy, O. Yaroshchuk, M. Serbina, R. Yamaguchi, Optics Express **20**, 3499 (2012).
26. J. Ma, Ya. Li, T. White, A. Urbas, Q. Li, Chem. Commun. **46**, 3463 (2010).
27. Y-C. Hsiao, C-Y. Tang, W. Lee, Optics Express **19**, 9744 (2011).
28. T. Yamamoto, Y. Tabe, H. Yokoyama, Thin Solid Films **509**, 81 (2006).
29. T. Yamamoto, Y. Tabe, H. Yokoyama, Colloids Surf. A **334**, 155 (2009).
30. V. Vinogradov, A. Khizhnyak, L. Kutulya, Y. Reznikov, V. Reshetnyak, Mol. Cryst. Liq. Cryst. **192**, 273 (1990).
31. S.N. Yarmolenko, L.A. Kutulya, V.V. Vaschenko, L.V Chepeleva, Liq. Cryst. **16**, 877 (1994).
32. P. Witte, J.C. Galan, J. Lub, Liq. Cryst. **24**, 819 (1998).
33. Yu. Reznikov, T. Sergan, Mol. Cryst. Liq. Cryst. **330**, 375 (1999).
34. M.I. Serbina, L.N. Lisetski, I.A. Gvozdovskyy, A.V. Koval'chuk, G.S. Chilaya, J. Funct. Mater. **17**, 449 (2010).
35. M. Mathews, R. Zola, S. Hurley, D. Yang, T. White, T. Bunning, Q. Li, J. Am. Chem. Soc. **132**, 18361 (2010).
36. I. Gvozdovskyy, O. Yaroshchuk, M. Serbina, Mol. Crys. Liq. Cryst. **546**, 202 (2011).
37. Q. Li, Y. Li, J. Ma, D.-K. Yang, T.J. White, T.J. Bunning, Adv. Mater. **20**, 1 (2011).
38. F.C.R. Grandjean, Hebd. Seances Acad. **172**, 71 (1921).
39. R. Cano, Bull. Soc. Fr. Mineral. Crystaleogr. **91**, 20 (1968).
40. M. Škarabot, M. Ravnik, S. Žumer, U. Tkalec, I. Poberaj, D. Babič, N. Osterman, I. Muševič, Phys. Rev. E **77**, 0317051 (2008).
41. P.R. Gerber, Z. Naturforsch. **35a**, 619 (1980).
42. I.I. Smalyukh, O.D. Lavrentovich, A.N. Kuzmin, A.V. Kachanski, P.N. Prasad, Phys. Rev. Lett. **95**, 157801 (2005).
43. K. Takahashi, M. Ichikawa, Y. Kimura, Phys. Rev. E **77**, 020703(R) (2008).
44. S. Joudkazis, M. Iwashita, T. Takahashi, S. Matsuo, H. Misawa, Appl. Phys. Lett. **74**, 3627 (1999).
45. Y. Iwashita, H. Tanaka, Phys. Rev. Lett. **90**, 045501 (2003).
46. T.A. Wood, H.F. Glesson, M.R. Dickinson, A.J. Wright, Appl. Phys. Lett. **84**, 4292 (2004).
47. U. Ognysta, A. Nych, V. Nazarenko, M. Škarabot, I. Muševič, Langmuir **25**, 12092 (2009).
48. S. Čopar, T. Porenta, V.S.R. Jampani, I. Muševič, S. Žumer, Soft Matter **8**, 8595 (2012).
49. S. Čopar, S. Žumer, Phys. Rev. Lett. **106**, 177801-4 (2011).
50. M. Kleman, J. Friedel, J. Phys. Colloq. **30**, C4-43 (1969).
51. T.J. Scheffer, Phys. Rev. A **5**, 1327 (1972).
52. Y. Bouligand, J. Phys. France **35**, 959 (1974).
53. I.I. Smalyukh, O.D. Lavrentovich, Phys. Rev. E **66**, 051703 (2002).
54. S. Čopar, S. Žumer, Proc. R. Soc. A **469**, 0204 (2013).